Optical Materials 32 (2010) 845–849

Contents lists available at ScienceDirect

Optical Materials

journal homepage: www.elsevier.com/locate/optmat

Invited Paper

Crystal growth and VUV luminescence properties of Er^{3+}- and Tm^{3+}-doped $LiCaAlF_6$ for detectors

Akira Yoshikawa [a,b,*], Takayuki Yanagida [a], Yuui Yokota [a], Akihiro Yamaji [a], Yutaka Fujimoto [a], Jan Pejchal [a,d], Valery I. Chani [a], Noriaki Kawaguchi [c], Sumito Ishizu [c], Kentaro Fukuda [c], Toshihisa Suyama [c], Martin Nikl [d]

[a] Institute of Multidisciplinary Research for Advanced Materials, Tohoku University, 2-1-1 Katahira, Aoba-ku, Sendai 980-8577, Japan
[b] New Industry Creation Hatchery Center (NICHe), Tohoku University, 6-6-10 Aoba, Aramaki, Aoba-ku, Sendai 980-8579, Japan
[c] Tokuyama Corporation Shibuya 3-chome, Shibuya-ku, Tokyo 150-8383, Japan
[d] Institute of Physics AS CR, Cukrovarnicka 10, 16253 Prague, Czech Republic

ARTICLE INFO

Article history:
Received 23 March 2010
Accepted 17 April 2010

Keywords:
VUV emission
Fluoride
Single crystal
Crystal growth from the melt
Er^{3+}
Tm^{3+}

ABSTRACT

Er- and Tm-doped $LiCaAlF_6$ (LiCAF) single crystals were grown by the micro-pulling-down (μ-PD) method. The crystals were transparent, 2.0 mm in diameter and 30–40 mm in length. Neither visible inclusions nor cracks were observed. Photoluminescence spectra of Er- and Tm-doped LiCAF were measured. Broad band emission due to the Tm^{3+} and Er^{3+} 5d–4f transitions dominated the spectrum at 163.5 and 165 nm respectively. These emissions had shortest wavelength among the fluoride crystal hosts ever reported at room temperature experiments. The vacuum ultraviolet (VUV) luminescent crystals are attractive as scintillators for radiation detectors, which employ photosensitive gases (such as TMAE or TEA) or photocathodes (such as CsI) sensitive mostly to VUV photons.

1. Introduction

Many fluoride crystals doped with rare earth elements (RE) such as Nd, Er, Tm show vacuum ultraviolet (VUV) emission [1–3]. The emission is due to parity-allowed radiative transitions from the lowest level of the excited $4f^{n-1}5d$ configuration to various lower lying $4f^n$ levels of RE^{3+}. These VUV emitting crystals are interesting as tunable VUV laser materials, e.g. $Nd:LaF_3$ [4,5]. In recent years, they were also considered as candidates for VUV scintillators for radiation detectors which employ photosensitive gases (such as TMAE or TEA) or photocathodes (such as CsI) sensitive mainly to VUV photons [6,7]. Tetrakis dimethyl amino ethylene (TMAE), trimellitic anhydride (TMA) and triethylamine (TEA) are the gases that are used as photosensitive gas additives, which produce photoelectrons with the energy of UV–VUV luminescence. The avalanche is started by the single electron ionized by the VUV luminescence. The ionization energies are 3.51 eV (353.2 nm) for TMAE, 5.97 eV (207.7 nm) for TMA, and 5.65 eV (219.5 nm) for TEA.

Therefore, RE^{3+}-doped crystals (RE = Nd, Er, Tm) became a subject of luminescence studies and applications in the field of VUV laser or scintillators. Especially, recent development of gas counter, such as μ-PIC, MSGC, and GEM [8–13] motivated us to perform the systematic study of VUV scintillators, which are indispensable part of such gas counter–scintillator detectors.

Vacuum photomultiplier tubes (PMTs) are used in various fields such as high-energy physics [14], medical imaging [15], and gamma-ray astronomy [16]. Since a flat, large-area PMT cannot be produced easily, a large number of PMTs are necessary in applications that require covering of large-area. On the other hand, a gas photomultiplier (GPM) [17,18] with both a photocathode and a structure for gas avalanche multiplication can be made with a very large area. This is because large-area micro-pattern gaseous detectors such as a micromegas [19], gas electron multiplier (GEM) [20–22], micro-pixel gaseous chamber (m-PIC), and micro-strip gas counter (MSGC) are available [23,24]. In addition to the above-mentioned photosensitive gas additives, some research groups had developed ultraviolet- (UV-) or visible-sensitive GPMs with CsI or bialkali photocathodes, respectively [17,18,25]. Although the bialkali photocathode has extremely strong chemical reactions, the CsI photocathode is easier to handle. An UV imaging detector with a CsI photocathode can be applied to material analysis research and liquid Ar/Xe scintillators. Thus, a gamma or hard X-ray imaging device that improves low

* Corresponding author at: Institute of Multidisciplinary Research for Advanced Materials, Tohoku University, 2-1-1 Katahira, Aoba-ku, Sendai 980-8577, Japan.
E-mail address: yosikawa@tagen.tohoku.ac.jp (A. Yoshikawa).

0925-3467/$ - see front matter © 2010 Elsevier B.V. All rights reserved.
doi:10.1016/j.optmat.2010.04.032

detection efficiency of gaseous detectors can be developed through coupling of such detectors with scintillating crystals.

In this study, we report the first study of the Er^{3+}- and Tm-doped LiCAF single crystal growth and related optical and luminescence characteristics.

2. Experimental procedure

2.1. Material design suitable for gas counter detector

TMAE, TEA photosensitive gases and CsI photocathodes start to operate with the emission shorter than 200 nm. The best efficiency obtained was bellow 150 nm. Therefore, the better detection efficiency of the gas counter detector is observed when the emission wavelength of the scintillating material is shorter.

In the stage of material design, we mainly revised the suitable crystalline hosts among fluoride-based materials. These crystals have wide band-gap of 9–11 eV. Therefore, they can be transparent around VUV region. Moreover, ability of their emission centers to perform transition between wide energy gaps was also examined.

Considering the requirement of wide band-gap and presence of suitable sites for RE^{3+} doping, we have chosen $LiCaAlF_6$ (LiCAF) single crystal as a host. LiCAF is a well-known host matrix for Ce^{3+} doping which has been studied from the view point of UV laser crystal [26,27]. Recent establishment of micro-pulling-down (μ-PD) method for the growth of fluoride systems [28] allowed us to perform systematic study of various fluorides for this purpose.

2.2. Crystal growth

Stoichiometric mixture of 4 N LiF, CaF_2, AlF_3, ErF_3 and TmF_3 powders (Stella Chemifa Co. Ltd.) was used as starting materials. Nominally, ErF_3 or TmF_3 were added to the $LiCaAlF_6$ host with the formula of $Li(Ca_{1-x}, RE_x)AlF_{6+x}$ (RE = Er, Tm), where $x = 0.01$. Crystal growth was performed from graphite crucible under Ar + CF_4 atmosphere using μ-PD apparatus with vacuum-tight systems. Thin platinum rod was used instead of the crystalline seed to initiate solidification at preliminary experiments. Further crystal growth experiments were carried out using the seed of undoped $LiCaAlF_6$ crystal obtained in the preliminary growth. The growth rate was 0.05–0.1 mm/min. The schematic diagram of a typical thermal setup as well as the baking procedure for fluoride crystal growth is given in Ref. [29].

2.3. Phase analysis

To identify the solidified phase, powder X-ray diffraction analysis was carried out in the 2θ range from 20° to 80° using the RIGAKU diffractometer (RINT2000). Measurements were performed in air and the X-ray source was Cu Kα, the accelerating voltage was 40 kV, and the tube current was 40 mA. All X-ray experiments were carried out at room temperature (RT). In order to identify the impurity phases, scanning electron microscope (SEM, S-3400N, Hitachi) equipped with energy dispersive X-ray (EDX, EX-250, Horiba) analysis was used.

2.4. Spectroscopic characterization

Transmission of the crystals was examined using Spectrofluorometer (Bunko-keiki Co. Ltd.), equipped with photo multiplier tube (PMT) (R6199, Hamamatsu), whose window was covered with salicylic acid. Emission spectra were also obtained from Spectrofluorometer (Bunko-keiki Co. Ltd.), equipped with VUV sensitive PMT (R374, Hamamatsu) and D_2 steady-state flash lamp as an excitation source. All the spectroscopic measurements in VUV region were performed under N_2 atmosphere.

3. Results and discussion

3.1. Crystal growth

The as grown crystals were 2.0–2.5 mm in diameter and around 30 mm in length. Neither visible inclusions nor cracks were observed. The as produced crystals appeared to be non-transparent. However, after negligible polishing of the surface, it was confirmed that all the defects were sited on the surface. Therefore, the as polished crystals were transparent (Fig. 1). During the crystal growth, some evaporation of LiF and AlF_3 was observed. For that reason, starting mixtures were prepared taking these losses into account. It is understood that the surfaces of the as grown crystals were covered with LiF and AlF_3 co-deposited during the growth runs.

The crystals were cut along the growth axis and polished with 0.3 μm diamond paste. The as obtained plates with the dimensions of $2.0 \times 7.0 \times 1.0$ mm^3 were used for the optical characterization.

3.2. Phase analysis

From the result of powder X-ray diffraction analysis, it was confirmed that the crystals were single phase materials with hexagonal crystal system, space group of $P\bar{3}1c$. No considerable difference between X-ray patterns obtained from undoped, Er-doped, and Tm-doped LiCAF was observed (Fig. 2).

Presence of inclusions of impurity phases was observed at the last parts of the crystal (end of the growth) as it is shown in Fig. 3. From the composition analysis of Er:LiCAF rod, two kinds of impurity phases were detected. One phase contained Ca and Er (Fig. 3(a)–(c)), but the other one was formed by Er only (Fig. 3(d)–(f)). Similar impurity phases were observed in Tm:LiCAF. We conclude that the impurity phases were RE:CaF_2 and REF_3 (RE = Er or Tm). These impurity phases were observed when the RE:LiCAF crystals were grown from stoichiometric melts. Formation of these secondary phases was result of enrichment of the melt with excess of RE due to its segregation. As the segregation coefficient of RE in LiCAF (Ca site) is less than 0.05 [30], the concen-

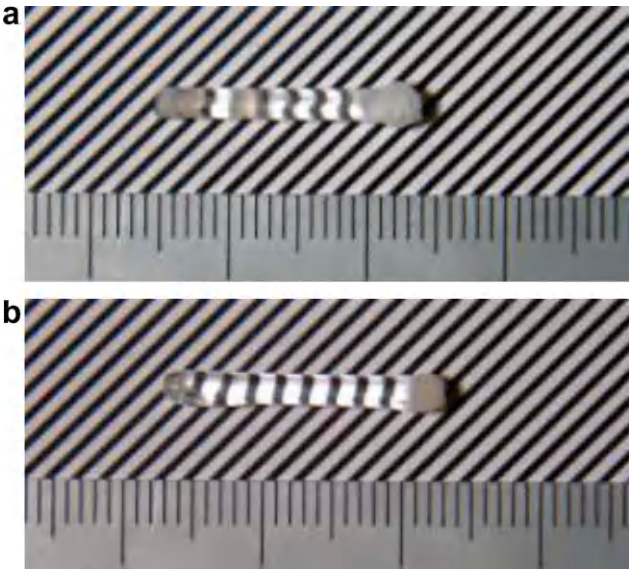

Fig. 1. View of (a) Er-doped and (b) Tm-doped $LiCaAlF_6$ (LiCAF) single crystals grown by the μ-PD method. Nominal composition was $Li(Ca_{0.99}, RE_{0.01})AlF_{6.01}$ (RE = Er, Tm).

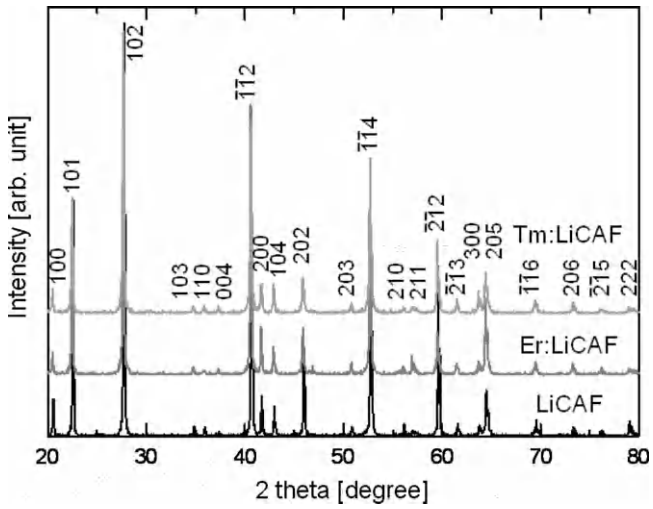

Fig. 2. Powder X-ray diffraction pattern of dispersed undoped, Er^{3+}-doped, and Tm^{3+}-doped LiCAF single crystals.

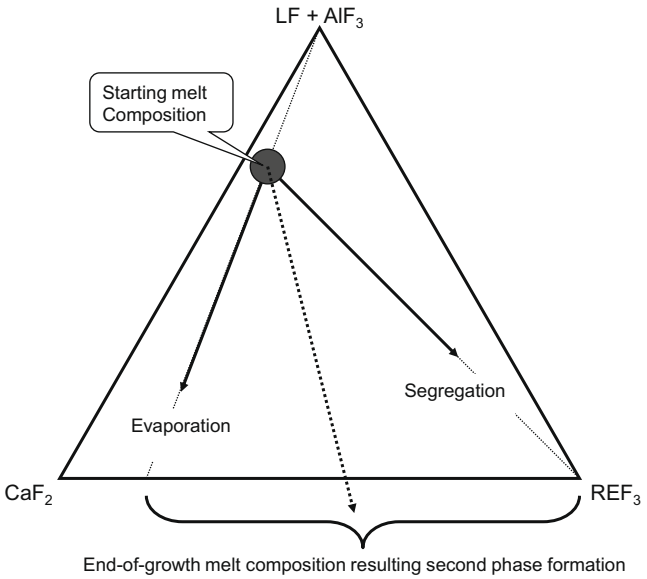

Fig. 4. Schematic phase diagram illustrating change of the melt composition during growth of RE-doped LiCAF crystal.

tration of RE in the melt was continuously increased as the growth was progressed. At some point of the growth run the concentration of RE became greater than that acceptable according to limit of the solid solution formation. Excess of Ca at the last part was caused by the evaporation of LiF and AlF during the growth process. As LiF and AlF_3 have lower vapor pressure than that of CaF_2, CaF_2 remains in some excess after the evaporation of LiF and AlF_3. CaF_2 can make solid solution with RE. Therefore, some amount of REF_3 reacted with the remained CaF_2 and formed RE:CaF_2 phase. However, as the amount of excess of REF_3 was significantly greater than that of remained CaF_2, formation of REF_3 was also observed. Schematic phase diagram illustrating change of the melt composition during growth of RE-doped LiCAF using μ-PD system is described in Fig. 4.

3.3. Spectroscopic characterization

Transmission spectra are shown in Fig. 5. Taking into account the description of the optical and luminescence transitions of Er^{3+} and Tm^{3+} in $LiYF_4$ host [31], the lowest energy spin-forbidden (so called high spin HS) $4f^n$–$4f^n$–15d transition of Er^{3+} and Tm^{3+} in LiCAF host was found at about 162–163 nm, while the spin-allowed (low spin LS) one was at about 154–155 nm. Another intense absorption peaks around 137–140 and 149–150 nm correspond to LS transitions to the higher 5d states.

The dominant reverse emission transition peaking around 163.5 nm (due to Er^{3+}) and around 165 nm (due to Tm^{3+}) in Fig. 6 can be ascribed to the HS transition into the lowest ground state level $^4I_{15/2}$ while the minor emission peaks are ascribed to the same HS transition into higher lying ^4I_x, $^4F_{9/2}$ and $^4S_{3/2}$ 4f levels.

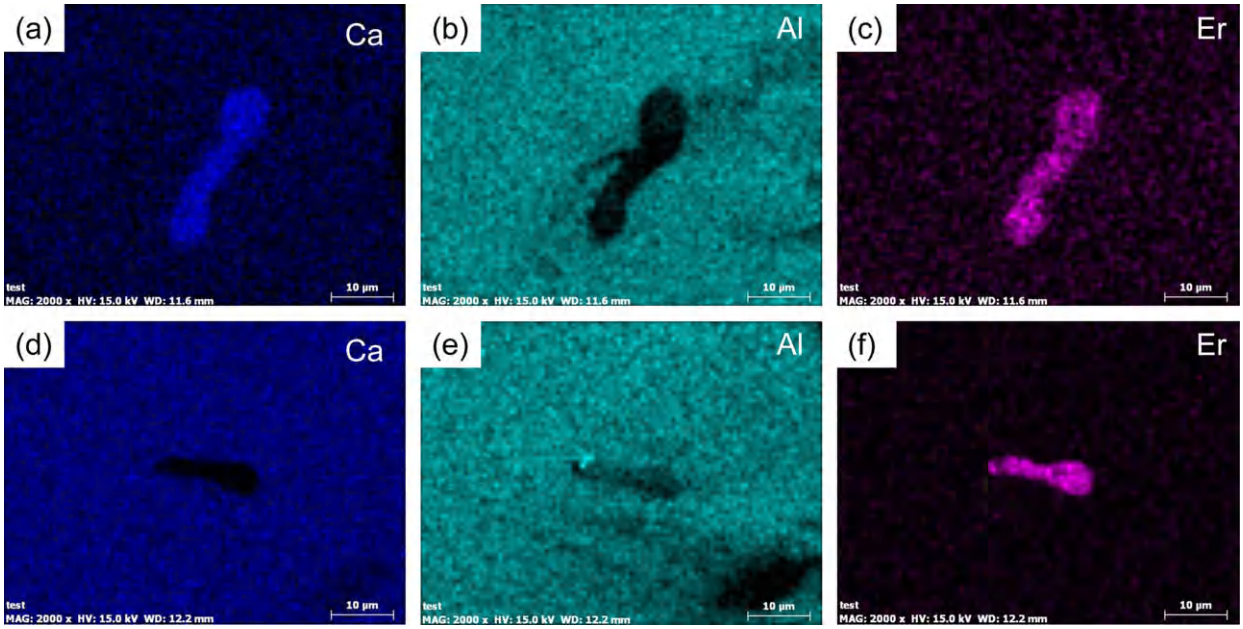

Fig. 3. Composition map of the impurity phases observed at the last part of the Er:LiCAF crystal.

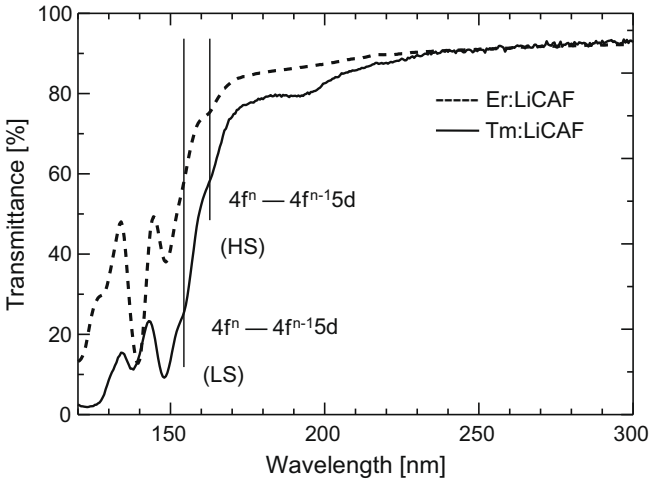

Fig. 5. Transmission spectra of Er^{3+}- and Tm^{3+}-doped LiCAF single crystals.

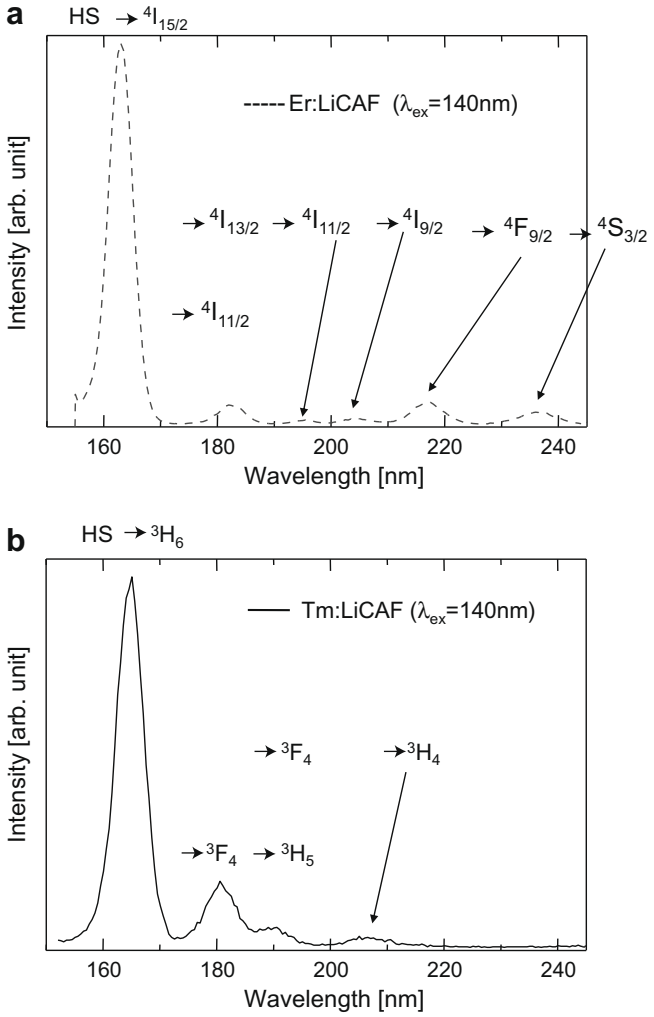

Fig. 6. Photoluminescence spectra of (a) Er^{3+}-doped and (b) Tm^{3+}-doped LiCAF single crystals excited by D_2 lamp. Excitation was performed at 140 nm, spectrally non-corrected. The level symbols indicated at the lower part of the pictures are those from the LS state.

The dominant emission peaks presented here are of the shortest wavelength ever reported among Er- and Tm-doped fluoride crystals [32–34] at room temperature. Thus, these crystals are attractive candidates for VUV scintillator applications in radiation detectors, which employ photosensitive gases (such as TMAE or TEA) or photocathodes (such as CsI) sensitive mainly to VUV photons. TMAE and TEA photosensitive gases and CsI photocathodes start to operate with the emission, which wavelength is shorter than 200 nm; however, the best efficiency is obtained at wavelengths bellow 150 nm.

4. Conclusions

Er- and Tm-doped LiCAF single crystals were grown by the μ-PD method. The crystals were transparent in the main volume and were 2.0 mm in diameter and 30–40 mm in length. Impurity phases were observed only at the last part of the crystals. These phases were identified as $RE:CaF_2$ and REF_3 (RE = Er or Tm). Dominant emission peaks due to spin-forbidden Er^{3+} and Tm^{3+} 5d–4f transition were detected around 163.5 and 165 nm, respectively. They were observed under D_2 lamp excitation at 140 nm. These emissions are of the shortest wavelength ever reported among Er- and Tm-doped fluoride crystals at room temperature. Therefore, we assume that these crystals are attractive for their application as VUV scintillators in radiation detectors, such as μ-PIC, MSGC and GEM, which employ photosensitive gases (such as TMAE or TEA) or photocathodes (such as CsI) sensitive mainly to VUV photons.

Acknowledgements

This work was partially supported by Ministry of Health and Welfare, Grant-in-Aid for the development of medical instruments and by Ministry of Education, Culture, Sports, Science and Technology of Japanese Government, Grant-in-Aid for Young Scientists (A), 19686001 (AY). Partial support form JSPS postdoctoral project P08055, joint project between JSPS and ASCR, and Czech GAAV project M100100910 are also gratefully acknowledged.

References

[1] K.H. Yang, J.A. DeLuca, Appl. Phys. Lett. 29 (1976) 499.
[2] P. Schotanus, C.W.E. van Eijk, R.W. Hollander, Nucl. Instrum. Methods A 272 (1988) 913.
[3] R. Visser, P. Dorenbos, C.W.E. van Eijk, A. Meijerink, H.W. den Hartog, J. Phys.: Condens. Matter 5 (1993) 8437.
[4] M.A. Dubinskii, A.C. Cefalas, E. Sarantopoulou, S.M. Spyrou, C.A. Nicolaides, R.Yu. Abdulsabirov, S.L. Korableva, V.V. Semashko, J. Opt. Soc. Am. B 9 (1992) 1148.
[5] R.W. Waynant, P.H. Klein, Appl. Phys. Lett. 46 (1985) 14.
[6] P. Schotanus, P. Dorenbos, C.W.E. van Eijk, R.W. Hollander, IEEE Trans. Nucl. Sci. 36 (1989) 132.
[7] P. Dorenbos, J.T.M. de Haas, C.W.E. van Eijk, J. Lumin. 69 (1996) 229.
[8] R. Chechik, A. Breskin, Nucl. Instrum. Methods A 595 (2008) 116–127.
[9] J.M. Maia, D. Mormann, A. Breskin, R. Chechik, J.F.C.A. Veloso, J.M.F. dos Santos, Nucl. Instrum. Methods A 580 (2007) 373–376.
[10] R. Oliveira, V. Peskov, F. Pietropaolo, P. Picchi, Nucl. Instrum. Methods A 576 (2007) 362–366.
[11] A. Takada, K. Hattori, S. Kabuki, H. Kubo, K. Miuchi, T. Nagayoshi, H. Nishimura, Y. Okada, R. Orito, H. Sekiya, A. Takeda, T. Tanimori, K. Ueno, Nucl. Instrum. Methods A 573 (2007) 195–199.
[12] K. Hattori, S. Kabuki, H. Kubo, S. Kurosawa, K. Miuchi, T. Nagayoshi, H. Nishimura, Y. Okada, R. Orito, H. Sekiya, A. Takada, A. Takeda, T. Tanimori, K. Ueno, Nucl. Instrum. Methods A 581 (2007) 517–521.
[13] H. Takahashi, K. Nishi, S. Paes, H. Niko, K. Fujita, P. Siritiprussamee, M. Ohno, B. Shi, M. Nakazawa, H. Toyokawa, S. Kishimoto, T. Ino, M. Furusaka, Nucl. Instrum. Methods A 579 (2007) 75–78.
[14] R. Dzhelyadin et al., The LHCb calorimeter detectors, Nucl. Instrum. Methods A 581 (2007) 384.
[15] C. Trotta et al., New high spatial resolution portable camera in medical imaging, Nucl. Instrum. Methods A 577 (2007) 604.
[16] Y. Chou et al., Observations of Cygnus X-1 with the EXITE2 hard X-ray balloon payload, ApJ. 618 (2005) 856.
[17] A. Breskin et al., Advances in gas avalanche photomultipliers, Nucl. Instrum. Methods A 442 (2000) 58.
[18] T. Francke et al., Novel position-sensitive gaseous detectors with solid photocathodes, IEEE Trans. Nucl. Sci. 49 (2002) 977.

[19] Y. Giomataris et al., MICROMEGAS: a high-granularity position-sensitive gaseous detector for high particle-flux environments, Nucl. Instrum. Methods A 376 (1996) 29.
[20] B. Ketzer et al., Performance of triple GEM tracking detectors in the COMPASS experiment, Nucl. Instrum. Methods A 535 (2004) 314.
[21] F. Sauli, GEM: A new concept for electron amplification in gas detectors, Nucl. Instrum. Methods A 386 (1997) 531.
[22] M. Inuzuka et al., Gas electron multiplier produced with the plasma etching method, Nucl. Instrum. Methods A 525 (2004) 529.
[23] A. Ochi et al., A new design of the gaseous imaging detector: micro pixel chamber, Nucl. Instrum. Methods A 471 (2001) 264.
[24] T. Nagayashi et al., Development of Î¼-PIC and its imaging properties, Nucl. Instrum. Methods A 525 (2004) 20.
[25] F. Tokanai et al., Development of gaseous PMT with micropattern gas detector, Nucl. Instrum. Methods A 610 (2009) 164.
[26] D.J. Spence, H. Liu, D.W. Coutts, Opt. Commun. 262 (2006) 238–240.
[27] Z. Liu, K. Shimamura, T. Fukuda, T. Kozeki, Y. Suzuki, N. Sarukura, Opt. Mater. 19 (2002) 123–128.
[28] A. Yoshikawa, M. Nikl, G. Boulon, T. Fukuda, Opt. Mater. 30 (2007) 6–10.
[29] A. Yoshikawa, T. Satonaga, K. Kamada, H. Sato, M. Nikl, N. Solovieva, T. Fukuda, J. Cryst. Growth 270 (2004) 427.
[30] K. Shimamura, S.L. Baldochi, N. Mujilatu, K. Nakano, Z. Liu, H. Ohtake, N. Sarukura, T. Fukuda, J. Cryst. Growth 211 (2000) 302.
[31] R.T. Wegh, A. Meijerink, Phys. Rev. B 60 (1999) 10820.
[32] P. Dorenbos, J.T.M. de Haas, C.W.E. van Eijk, J. Lumin. 69 (1996) 229–233.
[33] V.N. Makhov, N.M. Khaidukov, N.Yu. Kirikova, M. Kirm, J.C. Krupa, T.V. Ouvarova, G. Zimmerer, J. Lumin. 87–89 (2000) 1005–1007.
[34] D. Wisniewski, S. Tavernier, A.J. Wojtowicz, M. Wisniewska, P. Bruyndonckx, P. Dorenbos, E. van Loef, C.W.E. van Eijk, L.A. Boatner, Nucl. Instrum. Methods A 486 (2002) 239–243.